Comprehensive Kinetic Analysis of Influenza Hemagglutinin-Mediated Membrane Fusion: Role of Sialate Binding

Aditya Mittal and Joe Bentz
Department of Bioscience and Biotechnology, Drexel University, Philadelphia, Pennsylvania 19104 USA

ABSTRACT The data of Danieli et al. (*J. Cell Biol.* 133:559–569, 1996) and Blumenthal et al. (*J. Cell Biol.* 135:63–71, 1996) for fusion between hemagglutinin (HA)-expressing cells and fluorescently labeled erythrocytes has been analyzed using a recently published comprehensive mass action kinetic model for HA-mediated fusion. This model includes the measurable steps in the fusion process, i.e., first pore formation, lipid mixing, and content mixing of aqueous fluorescent markers. It contains two core parameters of the fusion site architecture. The first is the minimum number of aggregated HAs needed to sustain subsequent fusion intermediates. The second is the minimal number of those HAs within the fusogenic aggregate that must undergo a slow "essential" conformational change needed to initiate bilayer destabilization. Because the kinetic model has several parameters, each data set was exhaustively fitted to obtain all best fits. Although each of the data sets required particular parameter ranges for best fits, a consensus subset of these parameter ranges could fit all of the data. Thus, this comprehensive model subsumes the available mass action kinetic data for the fusion of HA-expressing cells with erythrocytes, despite the differences in assays and experimental design, which necessitated transforming fluorescence dequenching intensities to equivalent cumulative waiting time distributions. We find that HAs bound to sialates on glycophorin can participate in fusion as members of the fusogenic aggregate, but they cannot undergo the essential conformational change that initiates bilayer destabilization, thus solving a long-standing debate. Also, the similarity in rate constants for lipid mixing and content mixing found here for HA-mediated fusion and by Lee and Lentz (*Proc. Natl. Acad. Sci. U.S.A.* 95:9274–9279, 1998) for PEG-induced fusion of phosphatidylcholine liposomes supports the idea that subsequent to stable fusion pore formation, the evolution of fusion intermediates is determined more by the lipids than by the proteins.

INTRODUCTION

The molecular mechanism by which the envelope glycoprotein hemagglutinin (HA) of influenza virus induces membrane fusion has been intensely studied since it was the first fusion protein whose structure was solved (Wilson et al., 1981; Bullough et al., 1994) and its structure is related to other membrane fusion proteins (Skehel and Wiley, 1998). Furthermore, it is the only membrane fusion system for which there are quantitative data that can be used to deduce how many fusion proteins are required at the fusion site (Ellens et al., 1990; Melikyan et al., 1995; Danieli et al., 1996; Blumenthal et al., 1996; Bentz, 2000a). Thus, the architecture of its fusion site is being elucidated (Bentz et al., 1990; Bentz, 1993).

HA-mediated fusion subsumes at least four distinct intermediates, subsequent to close apposition of the membranes and the low pH-induced exposure of the HA2 N-terminus, which are defined by the assays that monitor their formation (Bentz, 1992, 2000a,b; Zimmerberg et al., 1994; Blumenthal et al., 1996; Hernandez et al., 1996; Chernomordik et al., 1997, 1998; Melikyan et al., 2000; Markosyan et al., 2000, 2001; Bentz and Mittal, 2000). Briefly, these intermediates are:

1. Aggregates of HA that form rapidly subsequent to acidification (Bentz, 2000a);
2. The first fusion pore that is defined by the first conductivity spike (2–5 nS) across the membranes;
3. The lipid channel, which is defined by the onset of lipid dye transfer to the target membrane, which might be due to hemifusion of the outer monolayers only;
4. The fusion site, which is defined by the onset of aqueous contents mixing (e.g., fluorophors) and the stable joining of the two membranes, a step required for nucleocapsid release for the virion.

Each of these steps will undoubtedly be subdivided in the future, as is being done now with pore evolution (Markosyan et al., 2001), and can be added to this kinetic model. However, the central problem will remain the same: how do we correlate these "communal" intermediates of the fusion process with the well-known "individual" conformations of HA fragments? (White and Wilson, 1987; Stegmann et al., 1990; Bullough et al., 1994; Chen et al., 1995; Yu et al., 1994; Hernandez et al., 1996; Carr et al., 1997; Böttcher et al., 1999). We believe that a rigorous kinetic analysis embracing the entire refolding landscape of HA will be essential.

Bentz (2000a) began the development of a comprehensive mass action model for HA-mediated fusion based upon the fusion intermediates listed above and used it to analyze the data of Melikyan et al. (1995) for first fusion pore formation between HA-expressing cells and ganglioside-containing planar bilayers. It was found that at least eight HAs must aggregate to form the fusogenic aggregate that

Received for publication 28 February 2001 and in final form 4 June 2001.
Address reprint requests to Dr. Joseph Bentz, Dept. of Bioscience/Biotechnology, Drexel University, 3141 Chestnut St., Philadelphia, PA 19104-2875. Tel.: 215-895-1513; Fax: 215-895-1273; E-mail: bentzj@drexel.edu.

0006-3495/01/09/1521/15 $2.00

TABLE 1 Comparison of essential experimental conditions for three distinct sets of data on HA-mediated membrane fusion

Data Source	Target Membrane	Temperature (°C)	pH	Fusion Stage*	Fusion Assay	Lag Time (s)† GP4f	HAb2	GP4/6
Melikyan et al. (1995)	Planar bilayers containing gangliosides	35–37	4.9	FP	Bilayer admittance measurement	182	53	n.d.
Danieli et al. (1996)	RBCs	28–29	5.0	Lipid mixing (≈LC)	R18 fluorescence dequenching	50	33	63
				FP	DiI fluorescence	5	n.d.	n.d.
Blumenthal et al. (1996)	RBC ghosts	37	~5.0	LC	DiI fluorescence dequenching	19	n.d.	n.d.
				FS	Calcein redistribution	39	n.d.	n.d.

*Intermediates in HA-mediated fusion. Appearance of each distinct intermediate is shown in Fig. 1. FP denotes the first fusion pore, LC denotes the lipid channel, and FS denotes fusion site.

†Lag times are defined by the x-intercept of the tangent to the fusion curve where the fusion rate is maximal (Bentz, 1992). Fusion curves for the data from Melikyan et al. (1995) are shown in Bentz (2000a), Fig. 1 there. Fusion curves for the data from Danieli et al. (1996) and Blumenthal et al. (1996) are shown in Figs. 2 and 3, respectively; n.d., not determined.

can sustain first fusion pore formation. Thus the minimal aggregate size is $\omega = 8$. Remarkably, only two or three of these HAs needed to undergo the slow "essential" conformational change required for first fusion pore formation. Thus, the minimal fusion unit is $q = 2$ or 3. This division of labor between those HAs that form the fusogenic aggregate and the subset of those HAs that form the minimal fusion unit is the core of this comprehensive fusion model. Both jobs are allowed by the model and the number of HAs required for each job is fitted from the data.

A comprehensive model must be able to bring all appropriate data into a coherent set of parameter estimates. Danieli et al. (1996) and Blumenthal et al. (1996) monitored the lipid mixing between HA expressing cells and fluorescently labeled RBC. They used different conditions, different assays, and different equations to arrive at different estimates for the number of HAs forming the "cooperative unit" or the fusion site. Blumenthal et al. (1996) correctly criticized the equation used in Danieli et al. (1996) as having no theoretical basis. In fact, both analyses were restrictive, in that a particular step of the process was assumed to be rate-limiting in advance and the fitting equations were designed for just that step. If no single step is rate-limiting, which our analysis suggests, then the parameters of overly simplified equations will be forced to accommodate the extra information in the data, blurring their physical meaning.

The comprehensive model applied here to their data makes no unproven assumptions about rate-limiting steps. We have assumed only that the data sets of Melikyan et al. (1995), Danieli et al. (1996), and Blumenthal et al. (1996) are representative of the different assays used to study the fusion of HA-expressing cells with target membranes. Hence, our focus is to determine whether this kinetic model can fit all the data and, if so, what can we learn about how the experimental design affects the fusion monitored.

Table 1 shows a synopsis of the different experimental setups used for the three studies. One major difference is that Melikyan et al. (1995) and Blumenthal et al. (1996) report waiting times for fusion intermediates to form between a single HA-expressing cell and a particular RBC, while Danieli et al. (1996) report the population averaged dequenching of fluorophor from labeled RBC into HA-expressing cells in suspension. We have derived a simple formula in Appendix B, which can translate the intensity data of Danieli et al. (1996) into its simplest waiting time form, thus all three data sets can be brought to the same basis for analysis.

MATERIALS AND METHODS

All data were recalibrated from original data kindly sent to us by Drs. Robert Blumenthal, Tsafi Danieli, and Judy White, as described below. Danieli et al. (1996) used stably transfected clones of the Japan strain of influenza virus (A/Japan/305/57) in 3T3 fibroblasts, denoted GP4f, HAb2, and GP4/6. Freshly drawn RBCs were labeled with octadecylrhodamine, R18, and bound to HA-expressing cells for 20 min at 25°C before washing. Fusion was triggered by lowering the pH of the above solution to 5.0 in a thermostatted cuvette at 28° to 29°C. Fluorescence dequenching of R18 from RBCs' membrane into the HA-expressing cell membrane was measured using a fluorometer equipped with a magnetic stirrer (LS-5B; Perkin-Elmer, San Jose, CA). We note that data from HAb2 cells treated with sodium butyrate were not used for this analysis.

Blumenthal et al. (1996) used only the GP4f cell line for their experiments. Human RBC ghosts double-labeled with DiI (C18-3) for lipid mixing, and calcein for content mixing, were monitored for fusion with the GP4f cells by multi-wavelength fluorescence video microscopy. A sudden small drop in RBC DiI fluorescence was often observed, well before the beginning of DiI redistribution, and was considered as an indicator membrane depolarization and, by inference, of the first fusion pore formation. Onset of DiI redistribution was taken as the waiting time of lipid mixing and onset of calcein redistribution was taken as the waiting time of aqueous contents mixing, which were determined by eye in Blumenthal et al. (1996). Using this system, a distribution of waiting times (for RBC ghosts) was obtained for the formation of the first fusion pore, the lipid channel, and the aqueous contents mixing. Not all cells showed all three outcomes, i.e., of the 76 cells that showed lipid dye spread, only 34 showed all three outcomes. For the 26 cells showing no clear drop in DiI fluorescence, it may have been too small to rise above the noise in the signal. For the 12 cells showing no calcein redistribution, it may be that lipid mixing was due to hemifusion (Chernomordik et al., 1998) or leakage of contents was too great (Shangguan et al., 1996). Because our model can treat each outcome independently, we used all of the data for fitting each step.

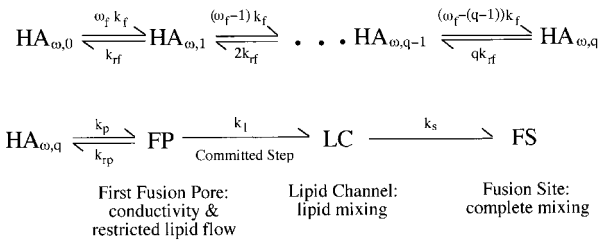

FIGURE 1 The comprehensive kinetic model for influenza hemagglutinin-mediated membrane fusion. Following protonation, the HA aggregate of size ω forms rapidly, denoted as $HA_{\omega,0}$. ω is the minimal size for a fusogenic aggregate and a lower bound of eight was found by kinetic analysis in Bentz (2000a), i.e., $\omega \geq 8$. ω_f denotes the number of the HAs within the fusogenic aggregate that can undergo the essential conformational change independently and identically with a rate constant of k_f. Thus, the overall rate constant for the first reaction would be $\omega_f k_f$. These conformational changes continue for each HA until q of them have occurred, $HA_{\omega,q}$. q is called the minimal fusion unit, as it equals the minimum number of HAs that have undergone the essential conformational change needed to stabilize the first high-energy intermediate for fusion. At this point, the fusogenic aggregate can transform to the first fusion pore, which is observed as the first conductivity across the apposed membranes. The first fusion pore, FP, evolves to the lipid channel, LC, demarked by mixing of lipids, which evolves to the fusion site, FS, demarked by aqueous contents mixing.

The kinetic model and multiparameter fitting of the fluorescence data

Fig. 1 shows the comprehensive kinetic model used for influenza hemagglutinin aggregation and fusion developed in Bentz (2000a) to analyze the first fusion pore kinetics found by Melikyan et al. (1995) between HA-expressing cells and ganglioside-containing planar bilayers. The model contains only those steps known to be essential for fusion. Following protonation, the HA aggregate forms rapidly, denoted here as $HA_{\omega,0}$, for an aggregate of ω HAs wherein none has yet undergone the essential conformational change. Although aggregation of HA is rapid, as shown in Bentz (2000a), that need not be the case for other fusion proteins; ω is the smallest aggregate size capable of achieving fusion, which was fitted as $\omega \geq 8$ in Bentz (2000a) for the data of Melikyan et al. (1995).

Although this reaction is theoretically reversible, we believe that the essential conformational change for HA is the formation of the extended coiled coil (Bullough et al., 1994; Carr et al., 1997; Shangguan et al., 1998; Skehel and Wiley, 1998), which appears to be irreversible under the conditions for fusion. Thus $k_{rf} = 0$ for our fits.

We have expanded the model slightly by having ω_f denote the number of the HAs within the fusogenic aggregate that can undergo an essential conformational change, independently and identically, with a rate constant of k_f. Thus, the overall rate constant for the first reaction would be $\omega_f k_f$. These conformational changes continue for each HA until q of them have occurred. Clearly, $q \leq \omega_f \leq \omega$. We will discuss below why this generalization is needed. Each of these parameters must be fitted by the data.

At this point, the fusogenic aggregate can transform to the first fusion pore, FP, which is observed as the first conductivity across the apposed membranes (Melikyan et al., 1995) or the sudden small drop in DiI fluorescence (Blumenthal et al., 1996). The minimal fusion unit, q, equals the number of conformationally changed HAs (i.e., their transduced free energy) needed to create and/or stabilize the first high-energy intermediate for fusion. The first fusion pore then evolves to the lipid channel, LC, demarked by the mixing of lipids, and then to the fusion site, FS, demarked by content mixing, if there is not too much leakage (Shangguan et al., 1996; Günter-Ausborn et al., 2000).

Data calibration: single cell waiting times versus population fluorescence dequenching

In the kinetic model, $\{FP(t)\}$ represents the average number of first fusion pores in the area of contact at time t. A Poisson distribution is used to obtain the probability at time t that a given cell has or has had one or more fusion pores (Bentz, 1992, 2000a):

$$N_{FP}(t) = 1 - \exp\{-[\{FP(t)\} + \{LC(t)\} + \{FS(t)\}]\} \quad (1)$$

The sum $\{FP(t)\} + \{LC(t)\} + \{FS(t)\}$ arises because $N_{FP}(t)$ is defined as the cumulant and an FS used to be an LC, which used to be an FP. By analogy, the waiting times for the first lipid mixing and contents mixing, as observed by Blumenthal et al. (1996), are given by:

$$\begin{aligned} N_{LC}(t) &= 1 - \exp\{-[\{LC(t)\} + \{FS(t)\}]\} \\ N_{FS}(t) &= 1 - \exp\{-[\{FS(t)\}]\} \end{aligned} \quad (2)$$

However, Danieli et al. (1996) measured fluorescence dequenching of labeled RBC bound to HA-expressing cells in a cuvette, i.e., a population average. They presented their lipid mixing assay results in terms of fluorescence dequenching, using a standard normalization,

$$I(t) = \frac{F(t) - F(0)}{F(\text{det}) - F(0)} \quad (3)$$

where $F(t)$ and $I(t)$ represent the absolute and relative fluorescence intensities respectively at time t or time 0, and $F(\text{det})$ is the fluorescence due to detergent lysis at the end of the experiment. This is a population measurement that presents two problems for fitting data. The first is using $F(\text{det})$ to approximate the fluorescence of complete lipid mixing. This is a common approach, but not one suitable for a rigorous kinetic analysis because it does not give the fraction of fused particles. The second problem is that the data cannot be compared directly with waiting times.

We have solved the first problem by recalibrating their intensity curves by replacing $F(\text{det})$ in Eq. 3 with $F(\infty)$, which is the maximum possible probe redistribution due lipid mixing only, i.e., not due to detergent lysis. $F(\infty)$ is the plateau value of lipid mixing fluorescence and was obtained by best-fitting the fluorescence dequenching curves to an approximate equation derived in Bentz (2000a) for first fusion pore formation:

$$F(t) = F(0) + 1 - \exp\{-A(1 - \exp\{-kt\})^B\} \quad (4)$$

For fitting lipid mixing here, the values of k and B have no rigorous significance, so we simply use it as a convenient equation for fitting A, since for the best fit, $F(\infty)$, is defined by

$$F(\infty) = F(0) + 1 - \exp\{-A\} \quad (5)$$

These fits were very good and agreed with visual estimates for the HAb2 and GP4f data, where plateaus were actually reached, while the GP4/6 curves required extrapolation.

The second problem, that of relating the population average dequenching with the fraction of fused cells, is partially solved in Appendix B, where it is shown that when the flow of probe to the target cell is fast compared with the time required for the next lipid channel to form, the appropriate relation is (Eq. B7):

$$I(t) = N_{LC}(t)(2 - N_{LC}(t)) \quad (6a)$$

or equivalently,

$$N_{LC}(t) = 1 - (1 - I(t))^{1/2} \quad (6b)$$

Where $N_{LC}(t)$ is defined in Eq. 2 relative to the kinetic model, Fig. 1.

Screening for "best fits"

Numerical integrations for the mass action kinetic model were done as in Bentz (2000a) using MATLAB (The Math Works) subroutine ODE23s. Curve-fitting was done using the fitting routine "fmins" of MATLAB. For the model in Fig. 1 we have found that theoretical data, generated from the model, are uniquely fitted by our algorithm. Thus, multiple fits here are due to experimental noise.

For any given data set the goodness-of-fit achieved by a particular set of kinetic parameters was quantitated by the root mean square error (rmse) between the data points and the numerically integrated theoretical curve. A minimum rmse value for each data set was obtained and "best fits" were defined as all sets of parameters that were visually indistinguishable from that of the minimal rmse fit. All data-fitting was exhaustive, i.e., the widest possible ranges of initial estimates for the parameters in the kinetic model were tested to assure that all best fits were found. This was confirmed by our finding that all best fits lay within a convex space in parameter space, as described below.

For Danieli et al. (1996) the lipid mixing data for the HAb2 cell line showed much more scatter than those for the GP4f and GP4/6 cell lines, making a simultaneous fitting of all three data sets too expensive computationally. Accordingly, we devised a three-step process to best-fit the data. First, the data for the for GP4f and GP4/6 cell lines were jointly fitted and a best-fit cutoff value of rmse = 2.85×10^{-2} was chosen, with an absolute minimum rmse of 2.76×10^{-2}, to collect the best-fit kinetic constants (k_f, k_p, k_l) and the number of fusogenic aggregates in the area of contact N_ω(GP4f),N_ω (GP4/6)). Second, for each of these chosen parameter sets, data for the HAb2 cell line were fitted solely for the number of fusogenic aggregates in the area of contact, denoted by N_ω(HAb2). The combined best-fit cutoff rmse value was calculated to be $\leq 5.20 \times 10^{-2}$, with an absolute minimum rmse = 4.76×10^{-2}. The third step was to exclude those fits for which $N_\omega(\text{GP4/6}) < 2$, i.e., two or more fusogenic aggregates were required within the area of contact, which we consider a weak assumption. N_ω(GP4/6) has the lowest surface density of the three cell lines, and hence the smallest number of available fusogenic aggregates.

The data from Blumenthal et al. (1996) were fitted in the same sequence as the appearance of fusion intermediates. First, for the distribution of first fusion pore waiting times, best fits for k_f, k_p, and N_ω(GP4f) were exhaustively generated. For each of these parameter sets, best fits for k_l were developed from the lipid mixing waiting times by providing a whole range of initial values for the rate constant for lipid channel formation in the model. This was followed by applying the same procedure to fit the rate constant for fusion site formation (aqueous fluorophor content mixing). Combined best-fit rmse values for all three fusion intermediates (FP, LC, and FS) were taken as $\leq 2.50 \times 10^{-2}$ for all data points, where the minimum rmse was 2.47×10^{-2}.

Cell constants

For all calculations the cell surface densities of HA on the GP4f cell line were taken as {GP4f} = 1600 HA/μm^2, {HAb2} = 1.6 × {GP4f} for the HAb2 cell line, and {GP4/6} = {GP4f}/1.6 for the GP4/6 cell line (Ellens et al., 1990; Danieli et al., 1996). The total area of GP4f and GP4/6 cell lines was taken as 1800 μm^2 and 2500 μm^2 for the HAb2 cell line (Ellens et al., 1990). The area of contact between a single RBC and an HA-expressing cell was taken as 38 μm^2 as measured by Danieli et al. (1996). We assumed 19 sialates per glycophorin (Pisano et al., 1993) and 2000–10,000 glycophorins per μm^2 on an RBC (Leikina et al., 2000; Marchesi et al., 1972).

RESULTS

It is important to observe that the overall kinetics from these three studies are rather different, as shown in Table 1 by the lag times, i.e., the x-intercept from the tangent at the maximal rate (Bentz, 1992). The lag times for the GP4f cells is the most complete set. For lipid mixing in Danieli et al. (1996) the lag time was ~50 s, while in Blumenthal et al. (1996) it was ~19 s. Much of this difference is due to the higher temperature, 37°C, Blumenthal et al. (1996) used as compared to 28–29°C used by Danieli et al. (1996). However, at the same temperature and a lower pH, Melikyan et al. (1995) show a lag time for first fusion pore formation that is ~35 times longer than that found in Blumenthal et al. (1996) for DiI depolarization.

Quantitative differences are due to experimental differences and to biological variation between these studies. We do not expect the comparison of rigorous fittings to completely agree. However, the job of a good comprehensive kinetic model is to show which parameters have similar values for the three studies, suggesting robust steps less sensitive to the experimental differences and which parameters have clearly different values, indicative of steps that depend strongly on details of the experiment.

The open symbols in Fig. 2 show the fluorescence dequenching due to lipid mixing curves from Danieli et al. (1996) for the three cell lines, recalibrated using Eqs. 3–5. The solid lines show a best fit to these data using Eq. 6, and all sets of kinetic parameters yielding a best fit gave visually indistinguishable curves. Over 2000 widely separated initial conditions were provided for fitting these data.

The symbols in Fig. 3 represent the waiting times for the fraction of GP4f cells that has shown membrane depolarization/first fusion pore formation (×), lipid mixing (□), and content mixing (+) from the data of Blumenthal et al. (1996). The solid lines show the best fit to these data, i.e., all sets of kinetic parameters yielding a best fit gave visually indistinguishable curves. Over 1000 widely separated initial conditions were provided for fitting these data.

Table 2 summarizes the fitted parameter ranges for both of these data sets. Also included are the ranges previously reported in Bentz (2000a) for the data of Melikyan et al. (1995) on first fusion pore formation with a ganglioside containing planar bilayer target, as measured by admittance changes. The most important result is that the data of Melikyan et al. (1995) and Danieli et al. (1996) require a minimal fusion unit of $q = 2$ or 3 to best fit the data. No other values of q, from 0 to 8, could fit all the data as well (i.e., no best-fit was found). By itself, the data of Blumenthal et al. (1996) allowed $q = 1$, 2, or 3 for best fits of the data for the GP4f cell line. However, the estimate for $q = 1$ is not reliable because data from Melikyan et al. (1995) or Danieli et al. (1996) for a single cell line could be best-fitted by other q values. Having data for more than one HA surface density significantly restricts the consensus parameter values. A major point of our analysis is that assuming all these data sets are reasonable implies that the consensus best fits are most reliable. The consensus value for the minimal fusion unit is $q = 2$ or 3.

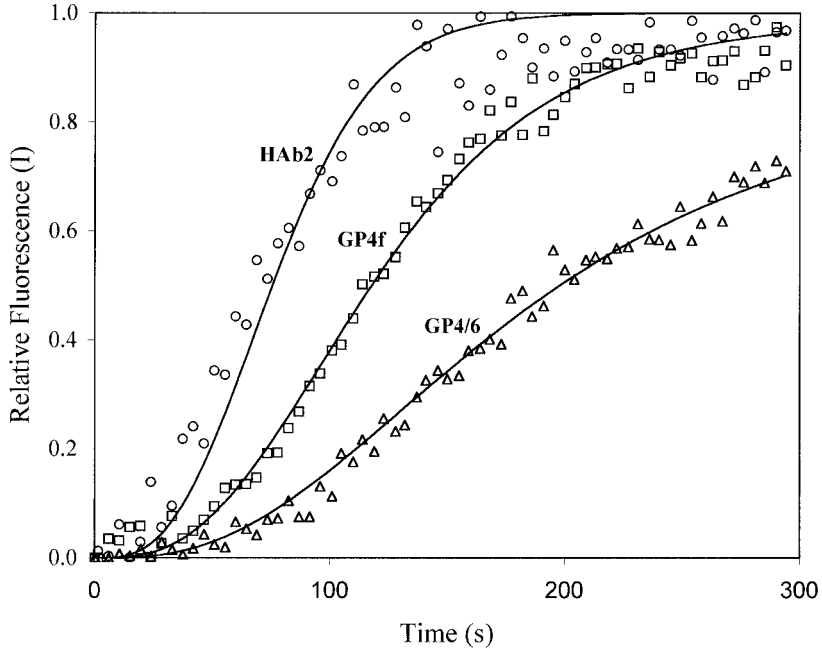

FIGURE 2 Lipid channel, LC, formation measured by Danieli et al. (1996) using R18-labeled RBCs fusing with HA-expressing cells. Open symbols show lipid mixing for three cell lines: GP4/6 (△), GP4f (□), and HAb2 (○). HAb2 cells express 1.6 times more HA/μm^2 than GP4f cells, and GP4f cells express 1.6 times more HA/μm^2 than GP4/6 cells (Danieli et al., 1996). Fusion is quantified as relative fluorescence due to lipid mixing (see Eq. 1). Solid lines show a typical best fit (see Results) obtained from multiparameter fitting of the data to the kinetic model. Other best fits can be obtained within the parameter ranges shown in Table 2.

The estimated range for the average rate constant for the first fusion pore formation k_p is in the range of 10^{-4}–10^{-5} s^{-1} if the minimal fusion unit $q = 2$. However, for $q = 3$, k_p is estimated either in the range of 10^{-5} s^{-1} or $\geq$0.5 s^{-1}, two widely disparate ranges. Bentz (2000a) noted that this showed the need for the analysis of other data to determine which range is correct. All three data sets analyzed here agree only on a single range for k_p, i.e., 10^{-4}–10^{-5} s^{-1}. This would also mean that the value of minimal fusion unit $q = 2$. Although such precision may appear unneeded, an independent analysis given below also suggests that $q = 2$.

For fitting the data of Danieli et al. (1996) alone, estimates for k_p and k_l were interchangeable because they control first-order processes in series with only the second step being measured, i.e., lipid mixing. The consensus from the three studies is shown in the table. The estimated range for the average rate constant for the lipid channel formation, k_l, is in the range of 10^{-3}–10^{-2} s^{-1}. The lower bound for the range of k_l found for the data of Blumenthal et al. (1996) alone is probably too low, due to having only one cell line tested. There is quite good agreement among the studies, which suggests a robust estimate for the kinetics of this step. From the data of Blumenthal et al. (1996), the value for the fusion rate constant was also estimated from Fig. 3 to be $k_S = 3 \times 10^{-2}$ s^{-1}. Lee and Lentz (1998) found similar values for the lipid mixing and content mixing between pure lipid vesicles (SUV) induced to fuse by PEG, which will be discussed below.

The rate constant for the essential HA conformational change, k_f, has absorbed most of the obvious kinetic difference among the three studies, discussed above and shown in Table 1 by the lag times. This step is the most sensitive to the experimental differences among the three studies. In the Discussion we will consider why this might be the case.

Confidence in the range of parameter values for best-fit sets requires that all possible best-fits are actually found. As in Bentz (2000a), we have found here that all best-fits are contained within a convex space of the universe of possible parameter values, as shown in the final column of Table 2. For the data of Melikyan et al. (1995), Bentz (2000a) found that all of the best-fit parameter sets could be fitted to the equation $k_p k_f^q N_\omega(\text{GP4f}) = 10^{-9.1\pm0.5}$ for $q = 2$ and $k_p k_f^q N_\omega(\text{GP4f}) = 10^{-9.5\pm0.1}$ for $q = 3$, as shown. In "parameter space," this relation defines a convex volume. This means we have the relevant ranges for all of the parameters. However, combinations of parameters that satisfy this relationship will yield good, but not always best, fits. Parts of this parameter space are inaccessible because they would require the number of HA ω-mers, denoted by N_ω, to exceed the available number of HAs in the area of apposition for the GP4f cell line. Similar relations hold for the best fits to the data of Danieli et al. (1996), when the value in the table equals $k_l k_p k_f^q N_\omega$(GP4f), and for the data of Blumenthal et al. (1996), when the value in the table equals $k_s k_l k_p k_f^q N_\omega$(GP4f). The parameter space values shown are mean values ±

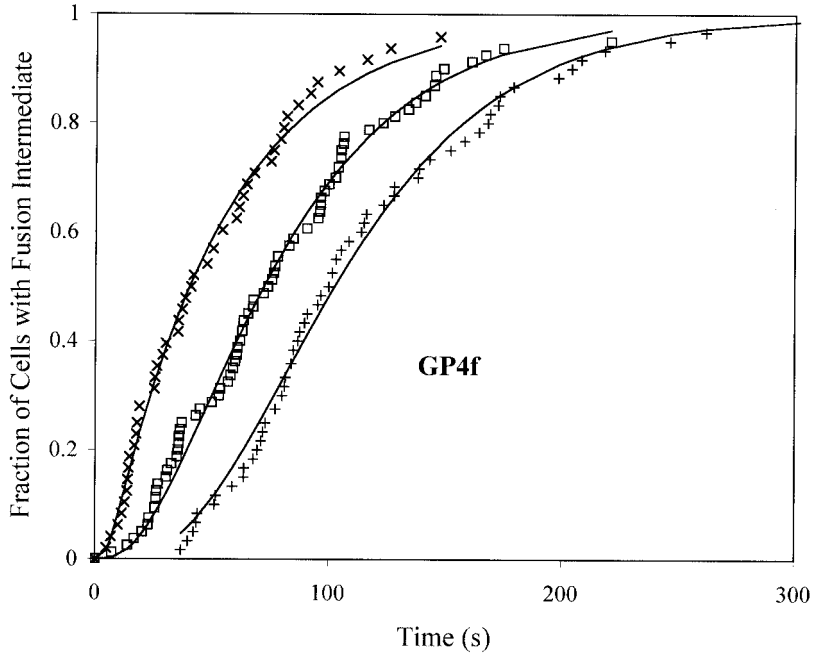

FIGURE 3 Fusion intermediates measured by Blumenthal et al. (1996) for double-labeled RBC ghosts fusing with GP4f cells. Symbols are the waiting time data after acidification, showing the cumulant fraction of cells that have achieved their first conductivity channel FP (×), their first indication for lipid channel formation LC (□), and their first indication for content mixing FS (+) as functions of time. Solid lines show a typical best fit obtained from multiparameter fitting of the data to the kinetic model (Eqs. 2–4). Other best fits can be obtained within the parameter ranges shown in Table 2.

TABLE 2 Comparison of the fitted parameter ranges for the data discussed in Table 1, using the mass action kinetic model for HA-mediated membrane fusion shown in Fig. 1

q*	Fusion Intermediate†	Protein k_f (s^{-1})‡	Fusion Pore k_p (s^{-1})‡	Lipid Channel k_1 (s^{-1})‡	$\frac{N_\omega(\text{HAb2})}{N_\omega(\text{GP4f})}$§	$\frac{N_\omega(\text{GP4f})}{N_\omega(\text{GP4/6})}$§	Parameter Space¶
2	FP‖ Melikyan et al. (1995)	$(0.3–2) \times 10^{-4}$	$(0.3–7) \times 10^{-4}$	n.d.	41 ± 2	n.d.	$10^{-9.1\pm0.5}$
	LC Danieli et al. (1996)	$(2–2.6) \times 10^{-2}$	$(4.5–8) \times 10^{-4}$	$(3–5) \times 10^{-2}$	2.92 ± 0.01	2.76 ± 0.01	$10^{-6.71\pm0.01}$
	LC Blumenthal et al. (1996)	$(2–2.5) \times 10^{-1}$	$(0.03–1) \times 10^{-4}$	$(2.5–2.6) \times 10^{-2}$	n.d.	n.d.	$10^{-6.08\pm0.002}$
3	FP‖ Melikyan et al. (1995)	$(0.4–2) \times 10^{-4}$	≥ 0.5	n.d.	39 ± 3	n.d.	$10^{-9.5\pm0.1}$
	LC Danieli et al. (1996)	$(1.5–2.2) \times 10^{-2}$	≥ 0.5	$(0.5–1.1) \times 10^{-3}$	2.95 ± 0.003	2.75 ± 0.002	$10^{-7.1\pm0.3}$
	LC Blumenthal et al. (1996)	$(3–3.1) \times 10^{-1}$	$(0.2–6) \times 10^{-5}$	$(2.5–2.6) \times 10^{-2}$	n.d.	n.d.	$10^{-6.41\pm0.002}$

*q denotes the minimal fusion unit. Only $q = 2$ or 3 could best fit the data. ω, the minimal aggregate size, was fixed at 8 from Bentz (2000a). For the data of Melikyan et al. (1995), where the target membrane was a ganglioside-containing planar bilayer, Bentz (2000a) assumed that all of the HAs in the fusogenic aggregate could undergo the essential conformational change, i.e., $\omega_f = \omega$. Here, for the data of Danieli et al. (1996) and Blumenthal et al. (1996), where the target membrane is a glycophorin on the RBC, we find that within the fusogenic aggregate, only those HAs not bound to sialates can undergo the essential conformational change, complementing the results of Leikina et al. (2000). Thus, the fitted value of k_f shown in Table 2 assumes that $\omega_f = 2$ or 3 for these data, i.e., $K_\sigma \geq 10^{-2}$ (molecules/μm^2)$^{-1}$, see Figs. 5 and 6. The initial fitting of the data with $\omega_f = \omega = 8$ gave fits for k_f that were ~5.5 times smaller for $q = 2$ and ~4.0 times smaller for $q = 3$. With these corrections all other parameters were insensitive to the value of ω_f.

†Fusion intermediates are defined in Fig. 1. FP denotes the first fusion pore, LC denotes the lipid channel, and FS denotes fusion site.

‡Best-fit ranges for the rate constants for the essential conformational change of HA, k_f, the first fusion pore formation, k_p, and the lipid channel formation, k_1. Results are shown for >25 best fits obtained in each case. Beyond the ranges shown either poor fits were obtained, or more ω-mer aggregates of HA were required in the area of apposition than were available for these cells, or the number of fusogenic aggregates in the area of apposition was <2.

§Average of ratio of the number of ω-mers in the area of apposition for the pairs of cell lines shown, for all best fits from the numerical integrations (±SD for >25 fits in each case).

¶Bentz (2000a) found that all of the best-fit parameter sets for the data of Melikyan et al. (1995) could be fitted to the equation $k_p k_f^q N_\omega(\text{GP4f}) = 10^{-9.1\pm0.5}$ for $q = 2$ and $k_p k_f^q N_\omega(\text{GP4f}) = 10^{-9.5\pm0.1}$ for $q = 3$, as shown. Similar relations hold for the best fits to the data of Danieli et al. (1996), when the value in the table equals $k_1 k_p k_f^q N_\omega(\text{GP4f})$, and for the data of Blumenthal et al. (1996), when the value in the table equals $k_s k_1 k_p k_f^q N_\omega(\text{GP4f})$. The parameter space values shown are mean values ± SD for >25 best fits obtained in each case.

‖Previously reported in Bentz (2000a).

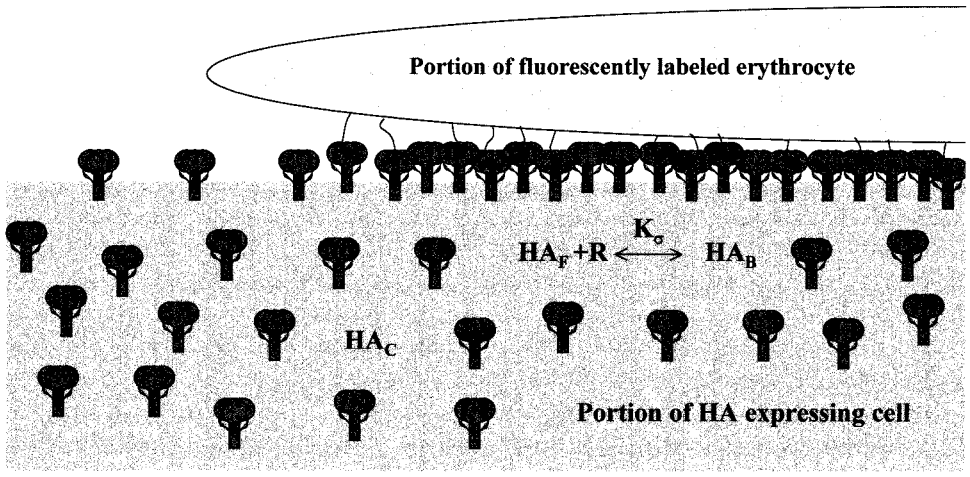

FIGURE 4 Accumulation of HAs in the area of apposition due to receptor binding. The portion of the HA expressing cell is shown with HA_c denoting HAs outside the area of apposition, at roughly the measured surface density for GP4f cells. The bound RBC (not to scale) is shown with glycophorin-HA connections accumulating HAs within the area of contact. The surface density of unbound HAs within the area of contact is denoted by HA_F, while HA_B denotes HA bound to glycophorin, which is denoted by R. The larger the binding constant K_σ, the more similar is HA surface density facing the RBC for all HA-expressing cell lines.

standard deviation for more than 25 best fits obtained in each case.

Bound HA can be a part of a fusogenic aggregate

Among the best fits, the particular values for N_ω(GP4f), N_ω(GP4/6), and N_ω(HAb2), the number of fusogenic aggregates on the GP4f, GP4/6, and HAb2 cells, ranged widely. However, their ratios were remarkably constant. In Bentz (2000a), it was found that this ratio for the data of Melikyan et al. (1995) was $N_\omega(\text{HAb2})/N_\omega(\text{GP4f}) = 41 \pm 2$ for $q = 2$ over hundreds of fits. Because the surface density (of HA) difference between HAb2 and GP4f cell lines was 1.6 (Ellens et al., 1990; Danieli et al., 1996), this ratio of 40 led to the conclusion that there were 8 or more HAs in the fusogenic aggregate Bentz (2000a,b).

The ratio of fusogenic aggregates for the lipid mixing data from Danieli et al. (1996) is more than 10-fold less and even more precise, i.e., 2.92 ± 0.01 for $q = 2$. Essentially the same ratio of fusogenic aggregates is found for the GP4f and GP4/6 cell lines, i.e., $N_\omega(\text{GP4f})/N_\omega(\text{GP4/6}) = 2.76 \pm 0.01$, for $q = 2$. These two cell lines also have an HA surface density ratio of 1.6 (Danieli et al., 1996). The standard deviation over all best fits ($n > 25$) is remarkably small. The reason for this reduction in the ratio of fusogenic aggregates is not because the cells are in suspension. A ratio of fusogenic aggregates of ~3 has also been observed for adherent HAb2 and GP4f cells fusing with R18-labeled RBCs observed by video microscopy (G. Melikyan, A. Mittal, and J. Bentz, unpublished observations).

This reduction in the ratio of fusogenic aggregates can be completely explained by HA binding to glycophorin on the RBC. This will cause the HAs to accumulate well above their average surface density within the area of contact between the RBC and the HA-expressing cell. This accumulation causes the absolute number of HAs within the area of contact to increase for both cell lines. However, the ratio of the total HA surface densities, between the GP4f and HAb2 cell lines, in the area of contact will decrease from 1.6 (no binding) to near 1 (all glycophorin sites bound and free HAs at the cell surface average). If the HAs bound to sialate can participate in the fusogenic aggregate in some way, then the ratio of fusogenic aggregates in the area of contact would diminish from 40, where there is insignificant binding as explained below, to a smaller number.

Fig. 4 illustrates a portion of the HA-expressing cell with HA_c denoting HAs outside of the area of apposition, at roughly the "measured" surface density (Ellens et al., 1990; Danieli et al., 1996). The bound RBC (not to scale) is shown with the glycophorin-HA connections accumulating HAs within the area of contact. We model the binding of HA to the glycophorin via its sialates in the simplest way:

$$HA_F + R \overset{K_\sigma}{\rightleftharpoons} HA_B$$

The larger the binding constant K_σ, the more similar the HA surface density facing the RBC for all HA-expressing cell lines, because the glycophorin (receptor) surface density is the same. The value of the binding constant K_σ will depend upon the sialate binding constant to the HA1 headgroup, the number of sialates per glycophorin, and any steric effects reducing the accessibility of the sialate to the binding site relative to the free sialate.

Calculating this binding effect is simple and is given in Appendix A. For our calculation, we assume that all of the

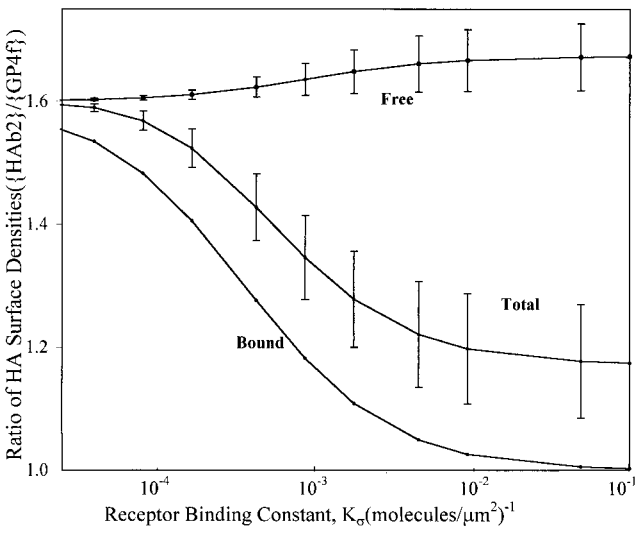

FIGURE 5 Dependence of ratio of surface densities on the receptor-HA binding constant in the area of apposition for the HA-expressing cells. Calculations were done using receptor surface densities of 2000, 5000, and 10,000/μm^2 based on existing data for glycophorins on RBCs (Marchesi et al., 1972; Leikina et al., 2000). Dots show the average ratios obtained from the calculations for these three surface densities and error bars are standard deviations. The separate ratios of free HA, bound HA, and total HA in the area of apposition are shown.

HAs on the cell surface are at equilibrium with the binding reaction to glycophorin in the area of contact. Leikina et al. (2000) made the assumption that no HAs could diffuse into the area of contact, which yields that essentially all of the HAs in the area of contact would be bound to sialates. If this assumption were correct, there would be no basis for fusion differences between the different cell lines. Given the mobility of HA (Ellens et al., 1990) and the accessibility of HAs within the area of contact to large proteolytic and glycolytic enzymes (Melikyan et al., 2000; Leikina et al., 2000), our assumption of free diffusion of HA into the area of contact is more reasonable. For all of our calculations, the surface density of free HAs within the area of contact, i.e., not bound to sialates, for the GP4f and HAb2 cell lines was always >85% and 94%, respectively, of the original surface density before binding. Thus, there are many free HAs. The fraction of HA bound within the area of contact was as high as 89% and 80%, respectively, due to accumulation of HAs.

What matters here is not the absolute values of HA, but the ratio between the two cell lines. Fig. 5 shows the graph of the calculated ratio of HA surface densities for HAb2 and GP4f cell lines in the area of RBC contact as a function of the binding constant K_σ. The separate ratios of free HA, bound HA, and total HA = bound + free are shown. This calculation does depend upon the surface density of glycophorin, which has been estimated from 2000 to 10,000/μm^2 (Marchesi et al., 1972; Leikina et al., 2000). We did the calculation for 2000, 5000, and 10,000 glycophorins/μm^2. Lines show the average of the calculated values for these three glycophorin surface densities and the bars show the standard deviation around this average. Although absolute amounts of bound HA depend on glycophorin surface density, the ratios between the two cell lines are rather insensitive. Thus, the true glycophorin surface density is not important for our analysis.

When the binding constant is near zero, the ratio of total HA is 1.6 in the area of contact, because all HA are free. When the binding constant $K_\sigma \geq 10^{-2}$ (molecules/μm^2)$^{-1}$, the ratio of total HA within the area of contact, between the HA2b/GP4f cell lines, is reduced to ~1.2. The binding constant of soluble sialate to soluble HA1 is well known, ≈1/(2.8 mM) (Sauter et al., 1989). However, the binding constant of membrane-bound HA to membrane-bound glycophorin, K_σ, has not been measured. Leikina et al. (2000) have estimated this value at $K_\sigma \approx 10^{-2}$ (molecules/μm^2)$^{-1}$, using a straightforward thermodynamic transformation and assuming that the sialate-HA binding is otherwise unchanged. Because their calculation did not include the fact that there are ~19 sialates per glycophorin (Pisano et al., 1993), their value is up to a 19-fold underestimate, i.e., $K_\sigma > 10^{-2}$ (molecules/μm^2)$^{-1}$.

Remarkably, the nucleation model for HA aggregation to fusogenic aggregates developed in Bentz (2000a) predicts that a reduction in ratio of fusogenic aggregates from 40 to 3 would require a reduction in the ratio of total HA in the area of contact from 1.6 to 1.2, for these two cell lines, as shown by Fig. 8 in Appendix A. These calculations suggest that the ratio of fusogenic aggregates we found here for the data of Danieli et al. (1996) is explained completely by the predicted accumulation of bound HAs within the area of contact, provided that the HAs bound to sialates can participate in fusion.

The minimal fusion unit requires free HA in the fusogenic aggregate

A fusogenic ω-mer aggregate of HAs can be composed of n_F free HAs and ($\omega - n_F$) bound HAs. Given that the ratio of fusogenic aggregates for HAb2 and GP4f cell lines fusing with RBCs from Danieli et al. (1996) is ~3, the solution to the nucleation equation (Eq. A6) is constrained for the value of n_F. Fig. 6 shows that the number of free HAs, n_F, required in the fusogenic aggregate depend mostly on the value of the binding constant, using Eq. A9. Dots show average values for the three glycophorin densities used (2000, 5000, and 10,000/μm^2) and error bars are for standard deviations for the different densities, as used in Fig. 5. It is clear once again that the actual value of glycophorin surface density is not crucial for these ratios. This constrained solution requires that the number of free HAs in the fusogenic aggregate, $n_F \approx 2$, when the binding constant $K_\sigma > 10^{-2}$ (molecules/μm^2)$^{-1}$. This is the same number as the consensus minimal fusion unit, $q = 2$. Thus, it seems clear that the minimal fusion unit, i.e., those HAs that undergo the essen-

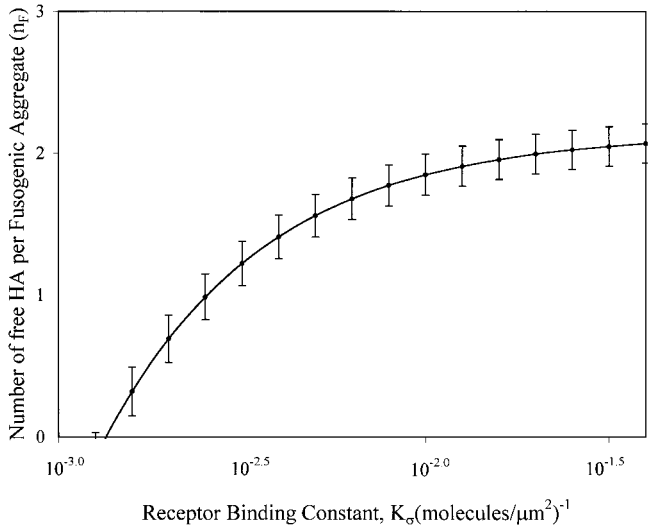

FIGURE 6 Number of free HA in the fusogenic aggregate as a function of the binding constant. A fusogenic ω-mer aggregate can be composed of n_F free and $(\omega - n_F)$ bound HA. Given that the ratio of fusogenic aggregates is ~3, the solution to nucleation reaction (Eqs. A6–A9) is constrained for values of n_F. This constrained solution requires that the number of free HAs in the fusogenic aggregate, $n_F \approx 2$, when the binding constant $K_\sigma > 10^{-2}$ (molecules/μm^2)$^{-1}$. Calculations were done using receptor surface densities of 2000, 5000, and 10,000/μm^2, as in Fig. 5. Dots on the curve show the averages obtained from these calculations for the three surface densities and error bars are standard deviations for the three different receptor surface densities, as in Fig. 5.

tial conformational change, must be composed of free HAs, while the remaining HAs in the fusogenic aggregate can be either free or bound.

For the data of Melikyan et al. (1995), where the target membrane was ganglioside-containing planar bilayer, Bentz (2000a) assumed that all of the HAs in the fusogenic aggregate could undergo the essential conformational change, i.e., $\omega_f = \omega$. Here, for the data of Danieli et al. (1996) and Blumenthal et al. (1996), for the target membrane glycophorin on the RBC, we find that only those HAs not bound to sialates can undergo the essential conformational change, complementing the results of Leikina et al. (2000). Hence, the fits needed to have $\omega_f = 2$ or 3. Operationally, we fitted the data twice, first with $\omega_f = \omega = 8$, to discover that the ratio of N_ω(HAb2)/N_ω(GP4f) had been reduced to ~3, compared with value of ~40 for the data of Melikyan et al. (1995). The second fitting used was $\omega_f = n_f = 2$, which gives the estimated parameter ranges reported in Table 2. Because the overall rate constant in the kinetic equations is $\omega_f k_f$, the values of k_f for the fits with $\omega_f = \omega = 8$ were ~5.5 times smaller for $q = 2$ and ~4.0 times smaller for $q = 3$. Other parameters were insignificantly affected. Thus, the 35-fold difference in lag times for fusion pore formation between Melikyan et al. (1995) and Blumenthal et al. (1996) translates to a 100-fold difference in the estimate for the rate constant k_f. Because the major difference between the two studies was the target membrane, we will consider below how this might affect k_f.

Membrane fusion site architecture cannot be predicted by lag times

Although our primary point is that an unrestricted comprehensive kinetic model for HA-mediated fusion shown in Fig. 1 can simultaneously fit these disparate data, we have also studied the predictive power of the equations used in the original studies. Blumenthal et al. (1996) fitted the cumulant waiting time between fusion pore formation and content mixing, i.e., the transition FP → FS using the notation of Fig. 1, to an equation for an n-mer aggregate of HAs executing independent and identical conformational changes with a rate constant k. The value of n and k were fitted. They only used one cell line, GP4f, and there is no obvious way to simultaneously fit data from other cell lines with their equation. They reported that the compound process of FP → FS required $n = 6$, which we confirmed using their Eq. 3. We also fitted their FP → LC data to their Eq. 3 and found that $n = 2.8$, while fitting the LC → FS data required $n = 1.7$. The model is not additive for some reason.

Danieli et al. (1996) used a version of a Hill plot of lag times to try to extract the "cooperative unit" of fusion, as have Stegmann et al. (1990) and Günter-Ausborn et al. (2000). We investigated the validity of the Hill plot analysis by simulating data for lipid mixing using our kinetic model and subjecting this simulated data to the Hill plot analysis used in Danieli et al. (1996). We used HA surface densities over the range of 1600 to 4000 HA/μm^2, ω was given the values of 6, 8, 9, 12, 18, and 24, and q was given the values of 1, 2, 3, 5, and ω. Thus, a wide range of possibilities were tested. The kinetic constants were $k_f = 10^{-4}$ s^{-1}, $k_p = 10^{-4}$ s^{-1}, and $k_l = 10^{-2}$ s^{-1}. Using other values within the ranges shown for the data in Table 2 would only change the time scales of the simulations and would not alter the conclusions we reach. Fig. 7 shows results of this analysis as the values of Hill coefficients (calculated as in Fig. 6 of Danieli et al., 1996) plotted against the various values of q used to simulate the data. The height of the bars shows the average value of the Hill coefficient for all the different values of ω used, 6 to 24, and error bars show the standard deviations. It is clear that ω, the minimal aggregate size, makes little difference to the value of the Hill coefficient. A Hill coefficient, by any simple definition of cooperativity, should reflect either the value of q or $(\omega - q)$ in our kinetic model. It correlates with neither in any predictive sense, as found before with a simpler kinetic model (Bentz, 1992). For all the values of q and ω used, the Hill coefficient was in the range of 1.25–3.51. The value of the Hill coefficient obtained by Danieli et al. (1996) was 2.83, i.e., within this range and implying that $q = 0$. These Hill plots have no validity for a kinetic process and no predictive power for the kinetic model used here.

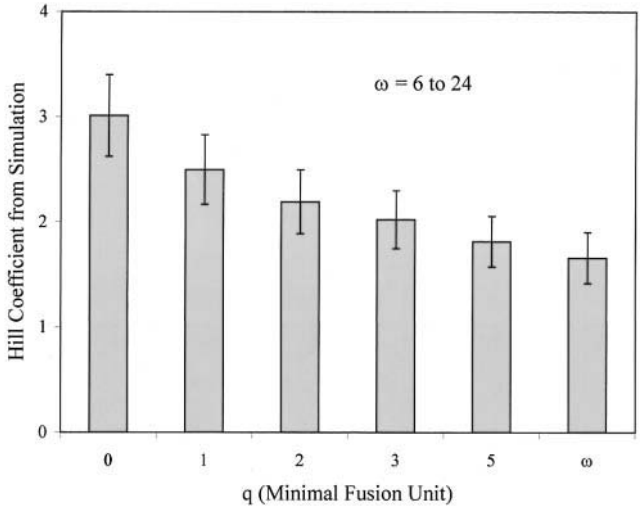

FIGURE 7 Hill coefficient dependence of the lag time for fusion on the minimal fusion unit size (i.e., the value of q). Using simulated data from the model in Fig. 1, lag times were found by calculating the x-intercept of the tangent to the fusion curve where the fusion rate is maximum (Bentz, 1992). Using these lag times, Hill coefficients were calculated exactly as in Fig. 6 of Danieli et al. (1996). Simulations used surface densities in the range of 1600–4000 HA/μm^2, ω was given the values of 6, 8, 9, 12, 18, and 24, and q was given the values of 1, 2, 3, 5, and ω. Histogram bars show the average value of the Hill coefficient for the different sizes of the fusogenic aggregate (i.e., the different values of ω) and error bars show the standard deviations.

DISCUSSION

It has long been suspected that there was more than one HA at the fusion site. Doms et al. (1985) noted that the initial fusion rate was more sensitive to pH than a single protonation site would predict, suggesting multiple protonations were required for fusion. However, because multiple protonation sites within a single HA trimer could also explain these data (Bentz et al., 1990), there was no resolution until fusion could be studied as a function of HA surface density, which is the only way to answer the question rigorously. Ellens et al. (1990) used the fusion of glycophorin-bearing liposomes with the GP4f and HAb2 HA expressing cell lines to show that more than one HA was required at the fusion site, i.e., $\omega \geq 2$. To obtain more precise estimates required a kinetic model of the event.

Obviously, a comprehensive kinetic model must contain all of the steps monitored during the fusion process. However, it must also recognize that to accomplish membrane fusion, several jobs are required of the membrane fusion proteins. A given fusion protein within a fusogenic aggregate may perform any one of these jobs, but there is no reason to believe that it can perform all of them (Bentz and Mittal, 2000). There should be a division of labor. This produces more parameters and, not surprisingly, more than one set of parameter estimates will give a best fit to the data, at least in part due to experimental noise. For the model in Fig. 1, we have found that theoretically simulated data are uniquely fitted by our algorithm, i.e., multiple fits to the data sets here are due solely to experimental noise. The fact that the model given in Fig. 1 can bring three very different sets of data into a single quantitative description suggests that it has just enough parameters to describe the fusion event for HA-expressing cells monitored by these assays.

The consensus best fits for the value of minimal fusion unit is $q = 2$ or 3. The estimate for the fusion pore formation rate constant, k_p, depends strikingly on the estimate for q, as was found in Bentz (2000a), where only the first fusion pore kinetics were analyzed. With the three data sets analyzed here, we find consistent estimates for k_p only if $q = 2$. Likewise, the analysis of sialate binding within the fusogenic aggregate showed that two free HAs are required. Thus, we find a very stringent result from two different approaches.

This analysis resolves a long-standing question. Many viral fusion systems have separate proteins to mediate the binding reaction to the target membrane (Bentz and Mittal, 2000). However, influenza HA contains both functions and there was controversy about whether the same HA can execute both functions (Ellens et al., 1990; Niles and Cohen, 1993; Alford et al., 1994; Stegmann et al., 1995; Millar et al., 1999; Leikina et al., 2000). Ellens et al. (1990) found that glycophorin-bearing liposomes bound equally well to both GP4f and HAb2 cells, implying the same number of HA-sialate contacts, but fused much more with the HAb2 cells. This proved that HAs need not be bound to sialate to induce fusion and suggested that a particular HA might not be able to perform both functions. Alford et al. (1994) found that influenza virions fused more slowly as the ganglioside surface density in the target liposomes was increased above 10 mol %, suggesting that HA bound to ganglioside lost the ability to sustain fusion. However, Millar et al. (1999) found that detergent-reconstituted virosomes could fuse with liposomes conjugated with Fab′ fragments directed against HA1 at or near the site of sialate binding. Simply being bound to a large membrane-bound molecule did not stop HA from eventually mediating fusion.

However, it is not known how well these Fab′ fragments mimic sialate binding. Leikina et al. (2000) found that soluble sialates inhibit the major conformational change of HA (X31 strain) and that RBC bound to HA(X31)-expressing cells fused faster following a neuraminidase treatment, i.e., with a reduction in HA-sialate contacts. The structural basis for sialate inhibition of the low pH conformational change of HA is unknown at this time. Ohuchi et al. (1999) reported in a review that deletion of glycosylation sites on HA1 of HA/USSR expressed on cells led to higher binding to RBC and reduced fusion of RBC. The IgG's used to generate the Fab′ fragments used in Millar et al. (1999) were screened to not inhibit the major conformation change of HA.

Now it is clear that the HAs bound to sialate on glycophorin may be part of the fusogenic aggregate. However, there must be at least 2 HAs within the fusogenic aggregate

unbound to sialates, as shown in Fig. 6, so that they can undergo the essential conformational change needed to create the fusogenic defect in a timely fashion. This suggests that the relatively weak HA-sialate binding constant could not evolve to a higher affinity, as that would inhibit its ability to mediate fusion. For fusion of the cells with ganglioside planar bilayers, where the ratio of fusogenic aggregates was 40 (Table 2), calculations suggest that on average fewer than one of the HAs within the aggregate are bound. This implies that HA binding to sialates is not necessary for fusion. It also implies that the binding constant of HA to ganglioside in a planar bilayer is at least two to three orders of magnitude smaller than that to glycophorin on RBC. This could be due to the difficulty for the HA1 binding site to reach sialates right next to the bilayer. This prediction can be tested. This is an example of the division of labor in fusion, i.e., there are two jobs for HAs within the fusion site and sialate bound HAs can fulfil only one of these jobs. However, there is more to the story.

We find it remarkable that the obvious kinetic differences in the original data, wherein the curves in Blumenthal et al. (1996) were faster than those in Danieli et al. (1996), which were faster than those in Melikyan et al. (1995), were parsed by the model into just one parameter: the rate constant for the "essential" conformational change, k_f. The low pH structure of the HA fragment shows two major conformational changes: the formation of the extended coiled coil and the helix-turn near the C-terminal end of the native coiled coil (Bullough et al., 1994). Both changes appear required for fusion (Bullough et al., 1994; Qiao et al., 1998; Skehel and Wiley, 1998). What is not known is which of these conformational changes is the "essential" one being monitored kinetically. That remains a model-specific definition.

The finding that only two of the eight or more HAs within the fusogenic aggregate need to undergo the essential conformational change for the first fusion pore to form is a severe constraint on the models for HA-mediated fusion. The model proposed in Bentz (2000b) and elaborated in Bentz and Mittal (2000) incorporated this constraint in the following way. It was proposed that after acidification, the fusogenic aggregate is formed from HAs with their fusion peptides embedded in the viral bilayer, due to the tension on the bilayer from the partial formation of the extended coiled coil (Kozlov and Chernomordik, 1998; Bentz and Mittal, 2000). The extraction of the fusion peptides by the formation of the extended coiled coil of two of these HAs was considered the essential conformational change. This would leave a hydrophobic defect in the center of the fusogenic aggregate, maintained by the "dam" of HA transmembrane domains and the remaining embedded fusion peptides. The helix-turn of one or two strands of the HA2 trimer would allow close approach of the apposed bilayers and place the hydrophobic kink at the helix-turn (Yu et al., 1994) over the hydrophobic defect, facilitating lipid flow (Bentz and Mittal, 2000).

This model provides a clear transduction of the energy released by the formation of the extended coiled coil to the formation of the first defect of fusion, as well as a need for a larger fusogenic aggregate ($\omega \geq 8$) than the number of HAs undergoing the essential conformational change ($q = 2$). The healing of this hydrophobic defect by lipid flow from the target membrane would create the first fusion intermediate, which would evolve into the first fusion pore and the subsequent intermediates. No other models have yet incorporated the constraint of the minimal fusion unit.

The large difference in the value of k_f between Blumenthal et al. (1996) and Melikyan et al. (1995), seen in Table 2, strongly suggests involvement of the target membrane. Because we have strong evidence now that the HAs specifically bound to sialates do not undergo the essential conformational change, there are two possible explanations. It could be that the bound HAs in the fusogenic aggregate simply make it easier for the free HA to undergo the essential conformational change, although how this would happen is unclear.

However, there is another possible explanation. The conformational change counts as "essential" only if it contributes toward making the initial defect that leads to the first fusion pore (Bentz, 2000a,b). If the conformational change had a probability of failure associated with it, call it p_F, for whatever reason, then the kinetic equations we use would replace k_f with $(1 - p_F)k_{f0}$, where k_{f0} would be the "true" rate constant for the HA protein conformational change (see Fig. 1). Although the "true" rate of a conformational change for a free HA may not depend upon the target membrane, this probability of failure certainly could. The fusogenic aggregates composed of only free HAs, i.e., with the ganglioside containing planar bilayer used in Melikyan et al. (1995), might have a much greater probability of failure than fusogenic aggregates against the glycophorin-bearing RBC, where all but two HAs are bound to glycophorin. Having most of the HAs in the fusogenic aggregate bound to sialates on glycophorin would hold the aggregate in place, because the lateral diffusion coefficient of these HAs tied to both membrane HAs would be sharply diminished. Thus, they would tend to hold the fusogenic aggregate together longer, which may well improve the odds of success in forming the first fusion pore. Measuring HA fusion under identical conditions to different target membranes could test this hypothesis.

Finally, we note that the rate constants for lipid channel formation and content mixing found here for HA-mediated fusion and those found by Lee and Lentz (1998) for PEG-induced fusion of small phosphatidylcholine liposomes are quite similar. This supports the idea that after stable fusion pore formation, the evolution of fusion intermediates is determined more by the lipids than the proteins (Chernomordik et al., 1997, 1998; Markosyan et al., 2000; Lentz et al., 2000; Bentz, 2000b; Haque et al., 2001). However, the rate constant for a first fusion pore-like event induced by

PEG is several orders of magnitude faster than what we measure here for HA-induced fusion, again showing that HA is intimately involved in its formation (Melikyan et al., 1997, 1999, 2000; Chernomordik et al., 1998, 1999; Markosyan et al., 2000, 2001; Bentz, 2000b).

The transfer of control from protein constraints to lipid constraints is likely to be gradual. The path between the first fusion pore and lipid mixing is clearly complex (Markosyan et al., 2001). Furthermore, a sequence of first-order processes, such as a sequence of intermediates from first fusion pore to lipid mixing, can be well-fitted as a single first-order process, as done here, without any one step being rate-limiting (Bentz, 1992). Comparison of the sequence as a function of HA surface density will be essential to understanding it (Bentz, 2000a).

APPENDIX A

Accumulation of HAs in the area of contact due to sialate binding to HA1

Let HA_F represent the HA in the area of target membrane contact not bound to the receptor (i.e., free HA) and HA_B represent the HA bound to glycophorin (denoted by "R"). The mass action surface binding of the glycophorin receptor with HA within the area of contact between the HA-expressing cell and the RBC is given by:

$$HA_F + R \overset{K_\sigma}{\rightleftharpoons} HA_B$$

The binding constant is defined as

$$K_\sigma = \frac{\{HA_B\}}{\{R\}\{HA_F\}} \tag{A1}$$

where braces represent the surface concentration in the units of molecules/μm^2.

Let HA_C represent the HA on cell surface outside the area of contact. We assume there is a uniform surface distribution of free or unbound HA on the cell surface, i.e., all of the HAs on the cell are at equilibrium with the binding reaction to glycophorin in the area of contact, which implies

$$\{HA_C\} = \{HA_F\} \tag{A2}$$

If we were to assume partitioning, i.e., $\{HA_F\} = K_c\{HA_C\}$, it would not affect our results significantly, so long as K_c is not too small. However, Leikina et al. (2000) assumed that no HAs could diffuse into the area of contact following initial cell-cell binding, which yields that nearly all HAs are bound by sialate. Given the mobility of HA (Ellens et al., 1990) and the accessibility of HAs within the area of contact with RBC to large proteolytic and glycolytic enzymes (Melikyan et al., 2000; Leikina et al., 2000), assuming free diffusion of HA into and out of the area of contact seems more reasonable. We did not consider the effect of glycophorin surface diffusion because its actual surface density does not affect our calculations significantly, as shown in Figs. 5, 6, and 8.

Let S denote the total surface area of an HA-expressing cell and δ denote the area of apposition between an RBC and the HA-expressing cell, then by mass balance

$$\begin{aligned} S\{HA_{Total}\} &= \delta(\{HA_F\} + \{HA_B\}) + (S - \delta)\{HA_C\} \\ &= \delta\{HA_B\} + S\{HA_F\} \end{aligned} \tag{A3}$$

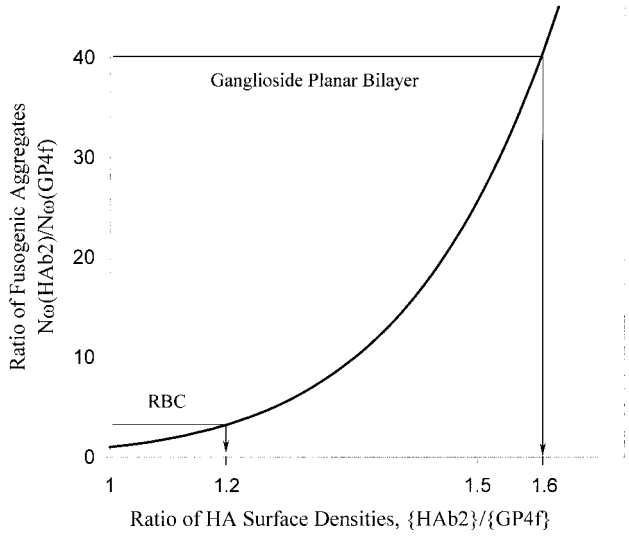

FIGURE 8 Calculated graph of ratio of fusogenic aggregates (for HAb2 to GP4f cell lines) as a function of the ratio of total HA surface densities in the contact area. The initial ratio of HA surface densities of 1.6 gave a ratio of fusogenic aggregates in the contact area as 40 (Bentz, 2000a). The measured value of the ratio of fusogenic aggregates using RBCs is ≈3, which implies that the initial ratio of surface densities is reduced to ~1.2. Calculations were done using the nucleation reaction, Eq. A7, using $n_F = \omega = 8$, i.e., all HAs in the fusogenic aggregates are free, as was the case in Bentz (2000a).

where $\{HA_{Total}\}$ is the surface density of all HA on the cell surface.

Let $\{R_o\}$ denote the total initial surface density of receptors on the erythrocyte and $\{R\}$ denote the surface density of free receptor after HA binding, then

$$\{R_o\} = \{R\} + \{HA_B\} \tag{A4}$$

For simplicity, we will assume that $\{R_o\}$ remains constant in the area of membrane contact. We will see below that the ratios of bound HAs for two cell lines are not very sensitive to the actual receptor surface density, so this is a weak assumption. Thus, given a binding constant K_σ, the amounts of bound and free HA can be calculated, as done in Fig. 5, using $\{R_0\}$ = 2000, 5000, and 10,000 glycophorins/μm^2 (Marchesi et al., 1972; Leikina et al., 2000).

To investigate the reduction of HA surface density ratios within the area of membrane contact observed in the lipid mixing data, we extended the nucleation model in Bentz (2000a) to include both free and receptor-bound HAs. The nucleation reaction forming a fusogenic aggregate of size ω, $X\omega$, which consists of n_F free HA and $(\omega - n_F)$ receptor-bound HA, can be written as

$$n_F HA_F + (\omega - n_F)HA_B \overset{K_n}{\longleftrightarrow} X_\omega$$

The nucleation binding constant is defined as

$$K_n = \frac{\{X_\omega\}}{\{HA_F\}^{n_F}\{HA_B\}^{\omega - n_F}} \tag{A5}$$

We assume that HA nucleation does not affect the sialate binding, which remains at equilibrium. Using Eq. A5, the number of fusogenic aggregates on a given cell is given by:

$$N_\omega \equiv \delta\{X_\omega\} = \delta K_n\{HA_F\}^{n_F}\{HA_B\}^{\omega - n_F} \tag{A6}$$

Thus the ratio of fusogenic aggregates on two cell lines is given by:

$$\frac{N_\omega(\mathrm{HAb2})}{N_\omega(\mathrm{GP4f})} = \left(\frac{\mathrm{HA_F}(HAb2)}{\mathrm{HA_F}(GP4f)}\right)^{\omega}\left(\frac{1 + K_\sigma\{\mathrm{HA_F}(GP4f)\}}{1 + K_\sigma\{\mathrm{HA_F}(HAb2)\}}\right)^{\omega - \mathrm{n_F}} \tag{A7}$$

which actually does not depend on the nucleation constant K_n.

Equation A7 can be solved for n_F for a fixed ratio of fusogenic aggregates (Table 2) as a function of K_σ and total receptor concentration R_o, as done in Fig. 6. The heavy curve shown in Fig. 8 is the ratio of fusogenic aggregates for other ratios of HA surface densities in the area of contact. The measured value for ratio of fusogenic aggregates for the RBC is ~3, which implies that the initial ratio of surface densities is reduced to ~1.2.

APPENDIX B

Predicting fluorescence dequenching from lipid mixing kinetics

We start from the treatment of Chen and Blumenthal (1989). The formation of the lipid channel, LC, demarks the beginning of lipid flow between the host and target membrane. We will consider the fusion of a fluorescently labeled RBC, with surface area A_E, to an HA-expressing cell with surface area A_C, where there are $m \geq 1$ RBC bound per cell on average. The equilibrium of this flow will depend upon the relative areas of the fusing cells. Here, we will assume that each RBC fuses independently and that the area of the cell patch available for probe dilution for that RBC is $A_P = A_C/m$, which is the eventual plateau value. This ignores some complications at the end of the dilution process, which require small corrections to the predicted fluorescence intensities at the cost of much more complex equations.

Fluorescence from a single RBC

For one RBC, the surface fraction of the fused product coming from this RBC is:

$$\sigma = \frac{A_E}{A_E + A_P} \tag{B1}$$

The average number of fluorescent probes on the RBC is denoted $N_E(0)$ before the lipid channel opens and $N_E(t)$ thereafter. It is essential to realize that each RBC will have different opening times, which we will treat explicitly below. Here we consider just the case of a given RBC.

Although lipid fluorophor labeling of RBC is heterogeneous, we will simply use the average value of fluorophors per RBC throughout. Also, to avoid a cluttered nomenclature, $N_E(0)$ etc. will denote these averages without explicit brackets. The number of probes transferred to the patch of cell available to this RBC will depend upon time and is denoted $N_P(t) = N_E(0) - N_E(t)$. At equilibrium, $N_E(\infty) = \sigma N_E(0)$ and $N_P(\infty) = N_E(0)(1 - \sigma)$. Chen and Blumenthal (1989) show formal equations for explicitly treating distributions, but if the labeling distributions are Gaussian-like, then the use of averages here should make little difference in the outcome. Thus, assuming average amounts of label per erythrocyte, the fluorescence intensity due to the probes from this RBC initially, finally and at time t are, respectively:

$$F(0) = N_E(0)Q\left[\frac{N_E(0)}{A_E}\right]$$

$$F(\infty) = N_E(\infty)Q\left[\frac{N_E(\infty)}{A_E}\right] + N_P(\infty)Q\left[\frac{N_P(\infty)}{A_P}\right]$$

$$= N_E(0)Q\left[\frac{\sigma N_E(0)}{A_E}\right]$$

$$F(t) = N_E(t)Q\left[\frac{N_E(t)}{A_E}\right] + N_P(t)Q\left[\frac{N_P(t)}{A_P}\right] \tag{B2}$$

$$= N_E(t)Q\left[\frac{N_E(t)}{A_E}\right] + (N_E(0) - N_E(t))Q\left[\frac{\sigma(N_E(0) - N_E(t))}{(1 - \sigma)A_E}\right]$$

where $Q[N/A]$ is the relative fluorescence of probes that are quenched by Förster energy transfer when there are N acceptors per area A (Wolber and Hudson, 1979; Düzgünes and Bentz, 1988). Thus, the relative fluorescence due to lipid mixing, normalized to the equilibrium or plateau value, i.e., not detergent lysis, is:

$$I(t) = \frac{F(t) - F(0)}{F(\infty) - F(0)}$$

$$= \frac{\eta(t)Q[\eta(t)a_0] + (1 - \eta(t))Q\left[\frac{(1 - \eta(t))}{(1 - \sigma)}\sigma a_0\right] - Q[a_0]}{Q[\sigma a_0] - Q[a_0]} \tag{B3}$$

where $\eta(t) = N_E(t)/N_E(0)$ and $a_0 = N_E(0)/A_E$.

At low concentrations of acceptor, where $Q[N/A] \approx 1 - \text{constant}*N/A$ (Hoekstra et al., 1984), Eq. B3 simplifies to:

$$I(t) = \frac{(1 - \eta(t))(1 + \eta(t) - 2\sigma)}{(1 - \sigma)^2} \tag{B4}$$

Interestingly, when dequenching is not linear, Eqs. B3 and B4 predict very similar values, within 10% relative error, due to the normalization. Thus the linear form is reasonable for us, given the scatter in the data.

Transforming the waiting time distribution to fluorescence dequenching

Now, Eq. B3 or B4 refer only to the dequenching of a particular RBC/cell fusion when the opening time is known. The real problem is that each of the RBC will have its lipid channel form at a different time and the ensemble fluorescence intensity would depend upon this distribution of opening times. This is why $I(t)$ does not equal the fraction of fused cells.

When LC(t) denotes the average number of lipid channels in the area of apposition between the RBC and the cell (Fig. 1), then we can use the Poisson distribution to obtain the fraction of RBC with one or more lipid channels, $N_{LC}(t)$ (Bentz, 1992, 2000a):

$$\mathrm{N_{LC}}(t) = 1 - \exp\{-\mathrm{LC(t)}\} \tag{B5}$$

This gives us the waiting time function used to fit the data of Blumenthal et al. (1996). To predict the cuvette fluorescence intensity from the waiting time distribution, we need to know how much of the probe has flowed through the channel since its formation, because that could be fast or slow, depending upon the probe.

If the time required for the probe to redistribute is fast compared with the time required for the next lipid channel to form, then the fraction of probe remaining on the RBC that have lipid channels will be $\sigma N_{LC}(t)$. The fraction of probe remaining on RBC that have not formed a lipid channel is obviously $1 - N_{LC}(t)$. Thus, in this case, the average fraction of probe on the RBC would be:

$$\langle\eta(t)\rangle = (1 - N_{LC}(t)) + \sigma N_{LC}(t) \tag{B6}$$

and the expected fluorescence from Eq. B4 would be,

$$I(t) = N_{LC}(t)(2 - N_{LC}(t)) \quad \text{(B7)}$$

using Eq. B6. This gives the simplest transformation between the measured fluorescence intensity and the number of RBC that have a lipid channel. If the lipid transfer is slow, then the fitting of $I(t)$ using Eq. B7 would underestimate the value for k_1 relative to a direct fitting of $N_{LC}(t)$ (Mittal et al., 2001).

We thank Robert Blumenthal, Tsafi Danieli, and Judy White for kindly providing the original data used here. We also thank Drexel University for the allocation of computer time.

REFERENCES

Alford, D., H. Ellens, and J. Bentz. 1994. Fusion of influenza virus with sialic acid-bearing target membranes. *Biochemistry.* 33:1977–1987.

Bentz, J. 1992. Intermediates and kinetics of membrane fusion. *Biophys. J.* 63:448–459.

Bentz, J. 1993. Viral Fusion Mechanisms. CRC Press, Boca Raton, FL.

Bentz, J. 2000a. Minimal aggregate size and minimal fusion unit for the first fusion pore of influenza hemagglutinin-mediated membrane fusion. *Biophys. J.* 78:227–245.

Bentz, J. 2000b. Membrane fusion mediated by coiled coils: a hypothesis. *Biophys. J.* 78:886–900.

Bentz, J., H. Ellens, and D. Alford. 1990. An architecture for the fusion site of influenza hemagglutinin. *FEBS Lett.* 276:1–5.

Bentz, J., and A. Mittal. 2000. Deployment of membrane fusion protein domains during fusion. *Cell Biol Int.* 24:819–838.

Blumenthal, R., D. P. Sarkar, S. Durell, D. E. Howard, and S. J. Morris. 1996. Dilation of the influenza hemagglutinin fusion pore revealed by the kinetics of individual fusion events. *J. Cell Biol.* 135:63–71.

Böttcher, C., K. Ludwig, A. Herrmann, M. van Heel, and K. Stark. 1999. Structure of the influenza haemagglutinin at neutral and at fusogenic pH by electron cryo-microscopy. *FEBS. Lett.* 463:255–259.

Bullough, P. A., F. M. Hughson, J. J. Skehel, and D. C. Wiley. 1994. Structure of influenza haemagglutinin at the pH of membrane fusion. *Nature.* 371:37–43.

Carr, C. M., C. Chaudhry, and P. S. Kim. 1997. Influenza hemagglutinin is spring-loaded by a metastable native configuration. *Proc. Natl. Acad. Sci. USA.* 94:14306–14313.

Chen, Y. D., and R. Blumenthal. 1989. On the use of self-quenching fluorophores in the study of membrane fusion kinetics. The effect of slow probe redistribution. *Biophys. Chem.* 34:283–292.

Chen, J., S. Wharton, W. Weissenhorn, L. Calder, F. Hughson, J. J. Skehel, and D. C. Wiley. 1995. A soluble domain of the membrane-anchoring chain of influenza virus hemagglutinin (HA2) folds in *Escherichia coli* into the low pH induced conformation. *Proc. Natl. Acad. Sci. USA.* 92:12205–12209.

Chernomordik, L. V., V. A. Frolov, E. Leikina, P. Bronk, and J. Zimmerberg. 1998. The pathway of membrane fusion catalyzed by influenza hemagglutinin: restriction of lipids, hemifusion, and lipid fusion pore formation. *J. Cell. Biol.* 140:1369–1382.

Chernomordik, L. V., E. Leikina, V. Frolov, P. Bronk, and J. Zimmerberg. 1997. An early stage of membrane fusion mediated by the low pH conformation of influenza hemagglutinin depends upon membrane lipids. *J. Cell. Biol.* 136:81–93.

Danieli, T., S. L. Pelletier, Y. I. Henis, and J. M. White. 1996. Membrane fusion mediated by the influenza virus hemagglutinin requires the concerted action of at least three hemagglutinin trimers. *J. Cell Biol.* 133:559–569.

Doms, R. W., A. Helenius, and J. White. 1985. Membrane fusion activity of the influenza virus hemagglutinin. The low pH-induced conformational change. *J. Biol. Chem.* 260:2973–2981.

Duzgunes, N., and J. Bentz. 1988. Fluorescence assays for membrane fusion. *In* Spectroscopic Membrane Probes, Vol. I, L. M. Lowe, editor. CRC Press Inc., Boca Raton, FL. 117–159.

Ellens, H., J. Bentz, D. Mason, F. Zhang, and J. M. White. 1990. Fusion of influenza hemagglutinin-expressing fibroblasts with glycophorin-bearing liposomes: role of hemagglutinin surface density. *Biochemistry.* 29:9697–9707.

Günter-Ausborn, S., P. Schoen, I. Bartholdus, J. Wilschut, and T. Stegmann. 2000. Role of hemagglutinin surface density in the initial stages of influenza virus fusion: lack of evidence for cooperativity. *J. Virol.* 74:2714–2720.

Haque, M. E., T. J. McIntosh, and B. R. Lentz. 2001. Influence of lipid composition on physical properties and peg-mediated fusion of curved and uncurved modelmembrane vesicles: "nature's own" fusogenic lipid bilayer. *Biochemistry.* 40:4340–4348.

Hernandez, L. D., L. R. Hoffman, T. G. Wolfsberg, and J. M. White. 1996. Virus-cell and cell-cell fusion. *Annu. Rev. Cell Dev. Biol.* 12:627–661.

Hoekstra, D., T. de Boer, K. Klappe, and J. Wilschut. 1984. Fluorescence method for measuring the kinetics of fusion between biological membranes. *Biochemistry.* 23:5675–5681.

Kozlov, M. M., and L. V. Chernomordik. 1998. A mechanism of protein-mediated fusion: coupling between refolding of the influenza hemagglutinin and lipid rearrangements. *Biophys. J.* 75:1384–1396.

Lee, J-K., and B. R. Lentz. 1998. Secretory and viral fusion may share mechanistic events with fusion between curved lipid bilayers. *Proc. Natl. Acad. Sci. U.S.A.* 95:9274–9279.

Leikina, E., I. Markovic, L. V. Chernomordik, and M. M. Kozlov. 2000. Delay of influenza hemagglutinin refolding into a fusion-competent conformation by receptor binding: a hypothesis. *Biophys. J.* 79: 1415–1427.

Lentz, B. R., V. Malinin, M. E. Haque, and K. Evans. 2000. Protein machines and lipid assemblies: current views of cell membrane fusion. *Curr. Opin. Struct. Biol.* 10:607–615.

Marchesi, V. T., T. W. Tillack, R. L. Jackson, J. P. Segrest, and R. E. Scott. 1972. Chemical characterization and surface orientation of the major glycoprotein of the human erythrocyte membrane. *Proc. Natl. Acad. Sci. U.S.A.* 69:1445–1449.

Markosyan, R. M., F. S. Cohen, and G. B. Melikyan. 2000. The lipid-anchored ectodomain of influenza virus hemagglutinin (GPI-HA) is capable of inducing nonenlarging fusion pores. *Mol. Biol. Cell.* 11: 1143–1152.

Markosyan, R. M., G. B. Melikyan, and F. S. Cohen. 2001. Evolution of intermediates of influenza virus hemagglutinin-mediated fusion revealed by kinetic measurements of pore formation. *Biophys. J.* 80:812–821.

Melikyan, G. B., H. Jin, R. A. Lamb, and F. S. Cohen. 1997. The role of the cytoplasmic tail region of influenza virus hemagglutinin in formation and growth of fusion pores. *Virology.* 235:118–128.

Melikyan, G. B., S. Lin, M. G. Roth, and F. S. Cohen. 1999. Amino acid sequence requirements of the transmembrane and cytoplasmic domains of influenza virus hemagglutinin for viable membrane fusion. *Mol. Biol. Cell.* 10:1821–1836.

Melikyan, G. B., R. M. Markosyan, M. G. Roth, and F. S. Cohen. 2000. A point mutation in the transmembrane domain of the hemagglutinin of influenza virus stabilizes a hemifusion intermediate that can transit to fusion. *Mol. Biol. Cell.* 11:3765–3775.

Melikyan, G. B., W. Niles, and F. S. Cohen. 1995. The fusion kinetics of influenza hemagglutinin expressing cells to planar bilayer membranes is affected by HA surface density and host cell surface. *J. Gen. Physiol.* 106:783–802.

Millar, B. M., L. J. Calder, J. J. Skehel, and D. C. Wiley. 1999. Membrane fusion by surrogate receptor-bound influenza haemagglutinin. *Virology.* 257:415–423.

Mittal, A., E. Leikina, J. Bentz, and L. V. Chernomordik. 2001. Kinetics of RBC fusion with influenza hemagglutinin-expressing cells as a function of technique. *Biophys. J.* 80(Part 2):417*a*. (Abstr.).

Niles, W. D., and F. S. Cohen. 1993. Single event recording shows that docking onto receptor alters the kinetics of membrane fusion mediated by influenza hemagglutinin. *Biophys. J.* 65:171–176.

Ohuchi, M., R. Ohuchi, and A. Matsumoto. 1999. Control of biological activities of influenza virus hemagglutinin by its carbohydrate moiety. *Microbiol. Immunol.* 43:1071–1076.

Pisano, A., J. W. Redmond, K. L. Williams, and A. A. Gooley. 1993. Glycosylation sites identified by solid-phase Edman degradation: O-linked glycosylation motifs on human glycophorin A. *Glycobiology.* 3:429–435.

Qiao, H., S. Pelletier, L. Hoffman, J. Hacker, R. Armstrong, and J. M. White. 1998. Specific single or double proline substitutions in the "spring-loaded" coiled coil region of the influenza hemagglutinin impair or abolish membrane fusion activity. *J. Cell Biol.* 141:1335–1347.

Sauter, N. K., M. D. Bednarski, B. A. Wurzburg, J. E. Hanson, G. M. Whitesides, J. J. Skehel, and D. C. Wiley. 1989. Hemagglutinins from two influenza virus variants bind to sialic acid derivatives with millimolar dissociation constants: a 500-MHz proton nuclear magnetic resonance study. *Biochemistry.* 28:8388–8396.

Shangguan, T., D. Alford, and J. Bentz. 1996. Influenza virus-liposomes lipid mixing is leaky and largely insensitive to the material properties of the target membrane. *Biochemistry.* 35:4956–4965.

Shangguan, T., D. Siegel, J. Lear, P. Axelsen, D. Alford, and J. Bentz. 1998. Morphological changes and fusogenic activity of influenza virus hemagglutinin. *Biophys. J.* 74:54–62.

Skehel, J. J., and D. C. Wiley. 1998. Coiled coils in both intracellular vesicle and viral membrane fusion. *Cell.* 95:871–874.

Stegmann, T., I. Bartoldus, and J. Zumbrunn. 1995. Influenza hemagglutinin-mediated membrane fusion: influence of receptor binding on the lag phase preceding fusion. *Biochemistry.* 34:1825–1832.

Stegmann, T., J. M. White, and A. Helenius. 1990. Intermediates in influenza induced membrane fusion. *EMBO J.* 13:4231–4241.

White, J., and I. A. Wilson. 1987. Anti-peptide antibodies detect steps in a protein conformational change: low-pH activation of the influenza virus hemagglutinin. *J. Cell Biol.* 105:2887–2896.

Wilson, I. A., J. J. Skehel, and D. C. Wiley. 1981. Structure of the haemagglutinin membrane glycoprotein of influenza virus at 3 Å resolution. *Nature.* 289:366–373.

Wolber, P. K., and B. S. Hudson. 1979. An analytic solution to the Forster energy transfer problem in two dimensions. *Biophys. J.* 28:197–210.

Yu, Y. G., D. S. King, and Y-K. Shin. 1994. Insertion of a coiled-coil peptide from influenza virus hemagglutinin into membranes. *Science.* 266:274–276.

Zimmerberg, J., R. Blumenthal, D. P. Sarkar, M. Curran, and S. J. Morris. 1994. Restricted movement of lipid and aqueous dyes through pores formed by influenza hemagglutinin during cell fusion. *J. Cell Biol.* 127:1885–1894.